LARGE-EDDY SIMULATIONS OF HIGH REYNOLDS NUMBER JETS WITH A SUITABLE SUBGRID-SCALE MODEL FOR SOLVER DEPENDENCY STUDY

M. Angelino, M. A. Moratilla-Vega, H. Xia and G. J. Page

Department of Aeronautical and Automotive Engineering, Loughborough University Loughborough, Leicestershire, LE11 3TU, United Kingdom

m.angelino@lboro.ac.uk

Abstract

Large-eddy simulations are performed of a turbulent round jet at Ma = 0.5 and 0.9. The solver dependency is explored on computationally affordable grids of 5 and 20 million grid points, by taking advantage of the consistency of the subgrid-scale σ-model. Three different solvers are tested. With all three, the computed mean and second-order fluctuating quantities of the turbulent near field compare favorably with measurements, for both Mach numbers and both grids, showing the strength of the σ-model in adapting to different flow conditions and grid refinements.

1 Introduction

In recent years, as the computing power continuously increases, Large-eddy simulations (LES) have become more and more feasible for the study of complex flows like turbulent jets (Bodony and Lele, 2008; Bogey and Bailly, 2006; Shur et al., 2005; Xia et al., 2009; Xia, 2015). Nevertheless, computational efficiency is still a priority. Numerical simulations of high Reynolds number turbulent jets can be strongly affected by the choice of the subgrid-scale model (Bogey and Bailly, 2003; Mahak et al., 2016) and of the solver (Tucker et al., 2006), especially if run on computationally affordable grids. The dependency on the solver is usually not easy to assess, since small numerical differences due to the code can be hidden by the subgrid-scale model, while the absence of a model, as in Implicit LES (ILES), can amplify those differences.

The choice of a suitable subgrid-scale model is therefore essential to identify solver dependency. Dynamic models (Germano et al., 1991) are usually considered a valid option, but they can be difficult to implement and to apply to complex flows. The model chosen for the present work is the σ-model (Nicoud et al., 2011), in which the subgrid-scale viscosity is defined as

$$\nu_{SGS} = (C_m \Delta)^2 \mathcal{D}_m(\mathbf{u}) \tag{1}$$

with

$$\mathcal{D}_m = \frac{\sigma_3(\sigma_1 - \sigma_2)(\sigma_2 - \sigma_3)}{\sigma_1^2} \tag{2}$$

where $\sigma_1 \geq \sigma_2 \geq \sigma_3 \geq 0$ are the three singular values of the velocity gradient tensor. The model constant reported in Nicoud et al. (2011), $C_m = 1.35$, has been used in this work. Unlike more standard models, like Smagorinsky (where $\mathcal{D}_m = \sqrt{2S_{ij}S_{ij}}$), the σ-model has the property to automatically vanish as soon as the resolved field is either two-dimensional or two-component, as in pure shear. In addition, it has the appropriate cubic behavior in the vicinity of solid boundaries without requiring any ad-hoc treatment. The model has been successfully adopted for jet noise prediction in Angelino et al. (2016), showing its strength in properly adapting to different grid refinements.

2 Numerical methods

The codes compared in this study are summarized in the following table:

	Code-A	Code-B	Code-C
code type	cell-centered	cell-vertex	cell-centered
continuity	density-based	density-based	pressure-based
time discret.	implicit	explicit	implicit
σ-model method	b	b	a

Table 1: Properties of the solvers

Code-A

Code-A (Xia, 2005) is an academic research code based on a cell-centered finite volume discretisation for arbitrarily unstructured meshes. To compute the inviscid flux, Roe's flux difference splitting approximate Riemann solver is employed at the interface between two neighboring control volumes:

$$\mathbf{F} = \frac{1}{2}(\mathbf{F}_L + \mathbf{F}_R) - \varepsilon \frac{1}{2} |\mathbf{A}| (\mathbf{Q}_R - \mathbf{Q}_L) \tag{3}$$

where $|\mathbf{A}| = \mathbf{M}|\mathbf{\Lambda}|\mathbf{M}^{-1}$ is the diagonalizing transform, $\mathbf{A} = \partial\mathbf{F}/\partial\mathbf{Q}$ the Jacobian, and ε is adopted as an additional parameter to control the amount of

upwinding (see Xia et al., 2009). The dual-time integral is employed with the outer physical time discretized by a three-level backward Euler scheme. This leads to second-order temporal accuracy. The inner pseudo time is advanced by a three-stage Runge–Kutta scheme. As the outer time is discretized implicitly, larger physical time steps are allowed thus increasing the efficiency compared with explicit time marching.

The σ-model has been implemented in it's method "b" formulation (Nicoud et al., 2011), which does not require the use of external scientific libraries. It finds the singular values of the resolved velocity gradient $\boldsymbol{g}$ through the calculation of three angles based on the invariants of the matrix $\mathbf{G} = \boldsymbol{g}^t\boldsymbol{g}$.

Code-B

Code-B (Moinier, 1999) is a density-based cell-vertex finite volume industrial code used for turbomachinery design. The second order flux calculation is based on the Roe scheme with a tunable parameter ε as in Code-A. For the temporal discretisation, a standard three-stage Runge-Kutta explicit algorithm is employed.

The σ-model has been implemented in it's method "b" formulation.

Code-C

Code-C (OpenFOAM) is a pressure-based compressible finite volume solver built on a combination of the pressure-implicit split-operator (PISO) and the semi-implicit method for pressure-linked equations (SIMPLE). The SIMPLE sub-iterations (1 in this case) allow a more stable convergence for larger time steps. The pressure equation is expressed in its *transonic* form as found in Demirdžić et al. (1993).

For the convective terms a blending of the central differencing scheme and the second order upwind scheme is applied through a local factor ε, with the same rationale as in the previous two codes.

Taking advantage of the existing scientific libraries in OpenFOAM, the σ-model has been implemented in its method "a" formulation (Nicoud et al., 2011), based on the direct calculation of singular values of the resolved velocity gradient $\boldsymbol{g}$ from the eigenvalues of the matrix $\mathbf{G} = \boldsymbol{g}^t\boldsymbol{g}$.

3 Case setup and flow conditions

The case studied is that of Set Point 3 and 7 of Tanna (1977), corresponding to cold jet conditions ($T/T_\infty \approx 1$ before the nozzle contraction), and acoustic Mach number at the jet exit $\mathrm{Ma} = U_j/a_\infty = 0.5$ and 0.9, respectively. The Reynolds number, based on the nozzle exit diameter D_j and jet exit velocity U_j, is around 5×10^5 and 10^6, respectively. The axisymmetric nozzle SMC000 (Bridges and Wernet, 2010) has a 2-inch exit diameter.

Solutions are obtained on multi-block structured grids with 5M and 20M cells. In order for the mesh refinement to be consistent in the whole domain, it follows an equal-ratio rule, i.e. the number of cells increases by $\sqrt[3]{4}$ times along all three directions. A detail of the nozzle exit for the 5M grid is depicted in Figure 1.

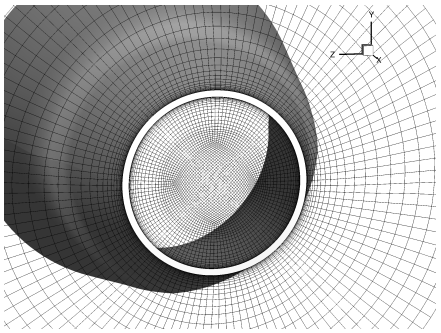

Figure 1: Detail of the nozzle exit for the 5M grid

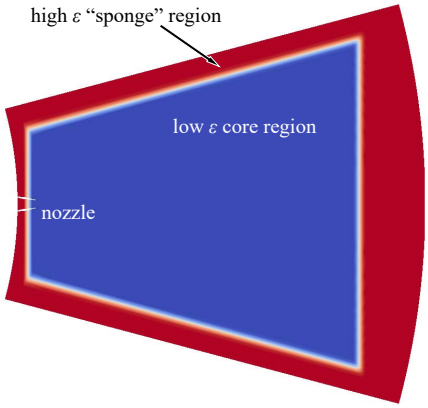

Figure 2: Distribution of the upwinding parameter ε

The computational domain consists of the upstream, jet inlet, farfield, and downstream boundaries. The domain is $50D_j$ long and expanded to a radial extent of $50D_j$ at the right end. On the nozzle solid wall, the no slip and adiabatic thermal conditions are applied.

Figure 2 gives the distribution of the upwinding parameter ε. Its maximum value of 1 corresponds to fully upwinded flux, which is used in the "sponge" zone to damp the acoustic reflections. Its minimal value needs to be tuned (≈ 0.1) to avoid numerical instabilities. A linear transition connects the two regions with the lowest and highest ε values.

4 Results and discussion

In order to demonstrate the superiority of σ-model compared with the traditional Smagorinsky-model, vorticity magnitude contours of the (x, y) plane, obtained with Code-B, are shown in Figure 3, for the 5M grid with $\mathrm{Ma} = 0.9$. Since there is no unsteady perturbations in the inflow conditions, the flow presents laminar behaviour inside the nozzle. However, by using the σ-model, the transition to a turbulent regimen occurs near the nozzle exit, as expected in high-Reynolds

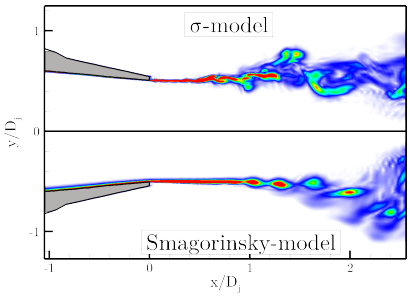

Figure 3: Vorticity magnitude contours of the (x, y) plane, 5M grid, Ma $= 0.9$, Code-B. Comparison of the σ-model and the Smagorinsky-model.

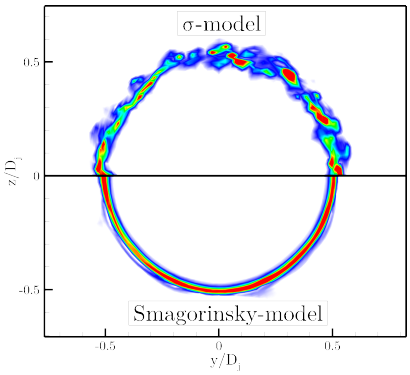

Figure 4: Vorticity magnitude contours of the (y, z) plane at $x/D_j = 0.75$, 5M grid, Ma $= 0.9$, Code-B. Comparison of the σ-model and the Smagorinsky-model.

number jets. On the contrary, with the Smagorinsky-model, this transition does not happen until $x/D_j = 1$, where highly coherent vortices appear. This should not occur for such a high Reynolds number.

Vorticity magnitude for a (y, z) plane at $x/D_j = 0.75$ can be seen in Figure 4. It is clear that, despite the coarse mesh used for this simulation, three-dimensional turbulent structures appear when the σ-model is used, whereas in the Smagorinsky-model case the flow is still two-dimensional. This clearly emphasis the fact that the σ-model behaves better than the Smagorinsky-model and, even in coarse meshes, is able to give a feasible representation of high-Reynolds number jets.

In the following paragraphs a detailed comparison of the results obtained with the σ-model with Code-A, Code-B and Code-C will be presented.

Figure 5 shows the Q-criterion coloured by velocity at Ma $= 0.9$ for the three solvers. They all show a large range of turbulent structures, where the smallest ones appear near the nozzle exit and, as the flow develops, these structures start to mix with each other creating larger ones. Code-A and Code-B show more regular oscillations in the initial shear layer, while Code-C yields a slightly faster transition from laminar to turbulent regimen in the shear layer.

Figures 6, 7 and 8 compare the centerline mean axial velocity and the centerline normal stress to experimental results (Bridges and Wernet, 2010; Zaman, 1986; Arakeri et al., 2003) at Ma $= 0.5$ with 5M grid points, Ma $= 0.9$ with 5M grid points, and Ma $= 0.9$ with 20M grid points, respectively. The agreement between the simulations and the experiments for the variables along the centerline is quite satisfactory, even for the 5M Ma $= 0.9$ case in which the mesh is quite coarse for the high Reynolds number of the simulation.

Similarly, Figures 9, 10 and 11 show the lipline behaviour of the normal stress. The peak that appears in the normal stress near the nozzle is possibly caused by the delay in the transition from laminar to turbulent regimen in the shear layer. In all the simulations this transition occurs slightly downstream from the nozzle lip. This is due to the fact that the inflow conditions that are used for these simulations do not include any characterisation of the turbulent levels in the boundary layer of the nozzle. However, Code-C has small numerical instabilities at the end of the nozzle, which trigger a faster transition. This explains as well the difference with the experiments, where the conditions that were used assure a turbulent regimen in the boundary layer of the nozzle.

Figures 12, 13 and 14 show shear stress radial profiles at four different locations near the nozzle exit, compared to experiments (Bridges and Wernet, 2010). For a clearer comparison, in each graph the value of the shear stress is shifted by 0.1 in the second profile, 0.2 in the third, and 0.3 in the fourth. These profiles confirm the sensitivity of the initial shear layer to the numerical differences of the solvers, which can be detected thanks to the vanishing of the σ-model in two-dimensional flows. For $x = 2D_j$ the discrepancy between the solvers and the experiments is the highest, which is in agreement with the highest value of the normal stress near the nozzle exist. However, for downstream location there is no real difference between the experiments and the simulations, which indicates that the development of the shear layer is not particularly affected by the initial peak of the stresses.

Further investigation is currently being conducted to assess the effect of inflow turbulence on the shear layer transition with the three solvers.

5 Conclusions

Large-Eddy Simulation results have been compared from three different solvers using the σ-model. All three solvers have proven to be very effective in capturing the overall behaviour of high Reynolds number jets, even with computationally affordable grids. Results are very consistent, with both grids of 5M and 20M grid points, and with Mach numbers 0.5 and 0.9. Slight discrepancies among the three solvers appear in the initial shear layer, where the transition seems to be driven by the solver numerics. The overall mean and fluctuating quantities, however, are code independent and compare favorably with measurements.

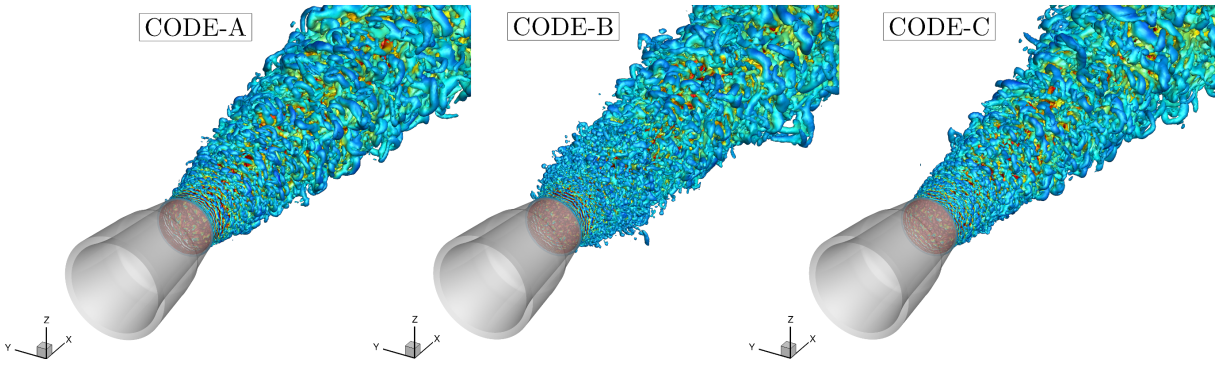

Figure 5: Q-criterion coloured by velocity for Ma = 0.9

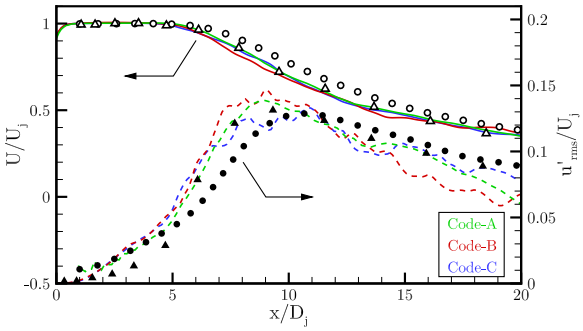

Figure 6: – centerline velocity, – – centerline normal stress, ◑ Bridges and Wernet (2010), ◭ Zaman (1986); Ma = 0.5; 5M cells.

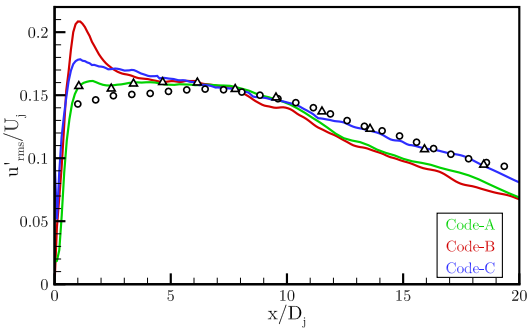

Figure 9: Lipline normal stress, ○ Bridges and Wernet (2010), △ Zaman (1986); Ma = 0.5; 5M cells.

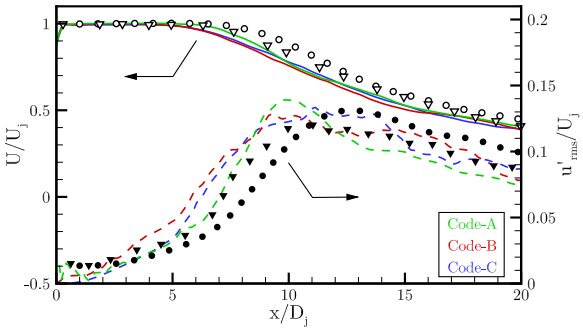

Figure 7: – centerline velocity, – – centerline normal stress, ◑ Bridges and Wernet (2010), ▽Arakeri et al. (2003); Ma = 0.9; 5M cells.

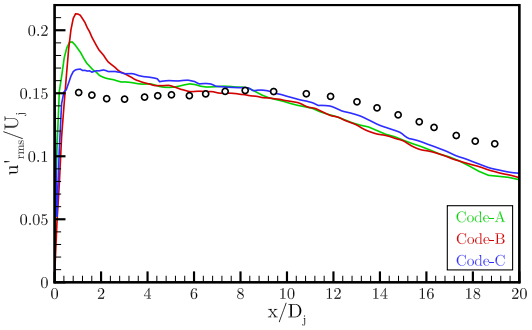

Figure 10: Lipline normal stress, ○ Bridges and Wernet (2010); Ma = 0.9; 5M cells.

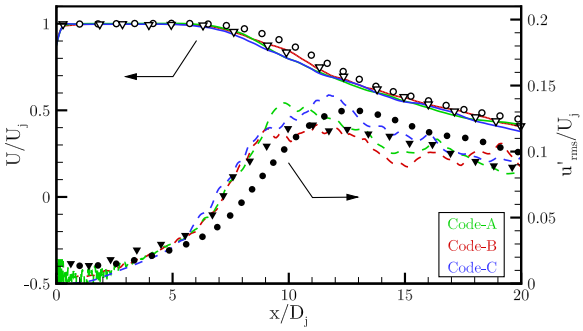

Figure 8: – centerline velocity, – – centerline normal stress, ◑ Bridges and Wernet (2010), ▽ Arakeri et al. (2003); Ma = 0.9; 20M cells.

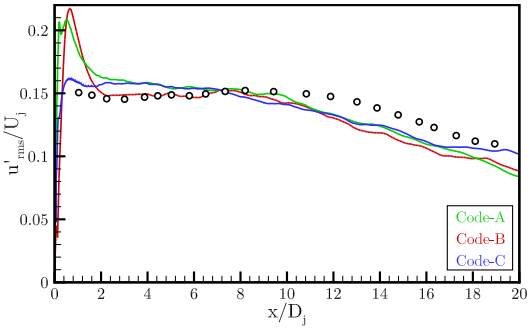

Figure 11: Lipline normal stress, ○ Bridges and Wernet (2010); Ma = 0.9 ; 20M cells.

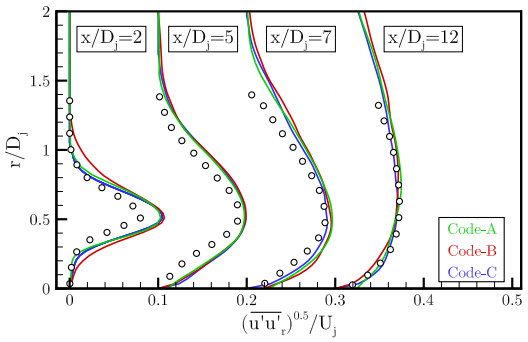

Figure 12: Shear stress radial profiles, ○ Bridges and Wernet (2010); Ma = 0.5; 5M cells.

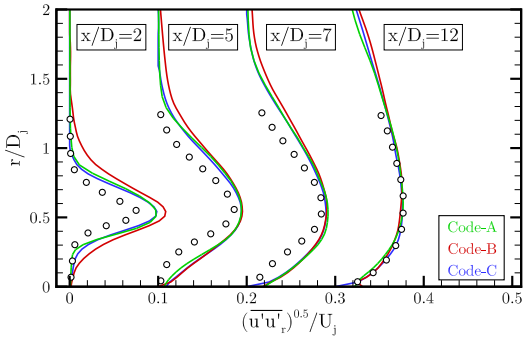

Figure 13: Shear stress radial profiles, ○ Bridges and Wernet (2010); Ma = 0.9; 5M cells.

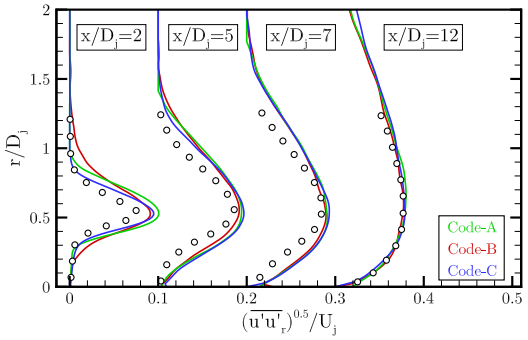

Figure 14: Shear stress radial profiles, ○ Bridges and Wernet (2010); Ma = 0.9; 20M cells.

Acknowledgments

The authors acknowledge the financial support from UK's Engineering and Physical Sciences Research Council (EPSRC) under grant number EP/M01391X/1. Computer time allocation units provided by the National ARCHER system (under project e377 and UK Turbulence Consortium project e01-Lough-Xia) are kindly acknowledged. The authors also thank HPC Midlands and Loughborough University's IT services for additional CPU time and support.

References

Angelino, M., Xia, H., Moratilla-Vega, M., and Page, G. (2016), Far-field Noise Prediction of Round and Serrated Jets with Increasingly Refined Grids. AIAA 2016-3047.

Arakeri, V. H., Krothapalli, A., Siddavaram, V., Alkislar, M. B., and Lourenco, L. M. (2003), On the use of micro-jets to suppress turbulence in a Mach 0.9 axisymmetric jet. *Journal of Fluid Mechanics*, 490:75–98.

Bodony, D. J. and Lele, S. K. (2008), Current Status of Jet Noise Predictions Using Large-Eddy Simulation. *AIAA Journal*, 46(2):364–380.

Bogey, C. and Bailly, C. (2003), LES of a High Reynolds, High Subsonic Jet: Effects of the Inflow Conditions on Flow and Noise. American Institute of Aeronautics and Astronautics.

Bogey, C. and Bailly, C. (2006), Computation of a high Reynolds number jet and its radiated noise using large eddy simulation based on explicit filtering. *Computers & Fluids*, 35(10):1344–1358.

Bridges, J. and Wernet, M. (2010), Establishing Consensus Turbulence Statistics for Hot Subsonic Jets. American Institute of Aeronautics and Astronautics.

Demirdžić, I., Lilek, ž., and Perić, M. (1993), A collocated finite volume method for predicting flows at all speeds. *International Journal for Numerical Methods in Fluids*, 16 (12):1029–1050.

Germano, M., Piomelli, U., Moin, P., and Cabot, W. H. (1991), A dynamic subgrid-scale eddy viscosity model. *Physics of Fluids A: Fluid Dynamics*, 3(7):1760.

Mahak, M., Moratilla-Vega, M., Page, G., and Xia, H. (2016), Assessment of WALE and Sigma(σ) Sub-Grid Scale Models for Jet Noise Prediction. AIAA 2016-2987.

Moinier, P. (1999), *Algorithm developments for an unstructured viscous flow solver*. PhD thesis, University of Oxford.

Nicoud, F., Toda, H. B., Cabrit, O., Bose, S., and Lee, J. (2011), Using singular values to build a subgrid-scale model for large eddy simulations. *Physics of Fluids*, 23(8):085106.

OpenFOAM. A free, open source CFD software package. Developed by OpenCFD Ltd at ESI Group and distributed by the OpenFOAM Foundation, *http://www.openfoam.org/*.

Shur, M., Spalart, P., and Strelets, M. (2005), Noise prediction for increasingly complex jets. Part I: Methods and tests. *International Journal of Aeroacoustics*, 4(3):213–246.

Tanna, H. (1977), An experimental study of jet noise part I: Turbulent mixing noise. *Journal of Sound and Vibration*, 50 (3):405–428.

Tucker, P., Coupland, J., Eastwood, S., Xia, H., Liu, Y., Jefferson-Loveday, R., and Hassan, O. (2006), Contrasting Code Performances for Computational Aeroacoustics of Jets. American Institute of Aeronautics and Astronautics.

Xia, H. (2005), *Dynamic Grid Detach-Eddy Simulation for Synthetic Jet Flows*. PhD thesis, University of Sheffield.

Xia, H. (2015), Turbulent jet characteristics for axisymmetric and serrated nozzles. *Computers & Fluids*, 110:189–197.

Xia, H., Tucker, P. G., and Eastwood, S. (2009), Large-eddy simulations of chevron jet flows with noise predictions. *International Journal of Heat and Fluid Flow*, 30(6):1067–1079.

Zaman, K. (1986), Flow field and near and far sound field of a subsonic jet. *Journal of Sound and Vibration*, 106(1): 1–16.